

Research paper

Advection-based tracking and analysis of salinity movement in the Indian Ocean

Upkar Singh^a, P.N. Vinayachandran^b, Vijay Natarajan^{a,*}^a Department of Computer Science and Automation, Indian Institute of Science, Bangalore 560012, India^b Centre for Atmospheric and Oceanic Sciences, Indian Institute of Science, Bangalore 560012, India

ARTICLE INFO

Keywords:

Multivariate temporal data
 Temporal tracking
 Oceanography
 Visualization
 Advection
 High salinity core
 Bay of Bengal

ABSTRACT

The Bay of Bengal (BoB) has maintained its salinity distribution over the years despite a continuous flow of fresh water entering it through rivers on the northern coast, which is capable of diluting the salinity. This can be attributed to the cyclic flow of high salinity water (≥ 35 psu), coming from Arabian sea and entering BoB from the south, which moves northward and mixes with this fresh water. The movement of this high salinity water has been studied and analyzed in previous work (Singh et al., 2022). This paper extends the computational methods and analysis of salinity movement. Specifically, we introduce an advection based feature definition that represents the movement of high salinity water, and describe algorithms to track their evolution over time. This method allows us to trace the movement of high salinity water caused due to ocean currents. The method is validated via comparison with established observations on the flow of high salinity water in the BoB, including its entry from the Arabian Sea and its movement near Sri Lanka. Further, the visual analysis and tracking framework enables us to compare it with previous work and analyze the contribution of advection to salinity transport.

1. Introduction

The Bay of Bengal (BoB) is a complex ocean system owing to its unique geographic setting and the combination of forcing by seasonally reversing monsoon winds and large quantity of freshwater supply to the bay from river runoff and rainfall (Shetye et al., 1996; Rao and Sivakumar, 2003; Behara and Vinayachandran, 2016). The flow of fresh water from rivers in the northern coast is capable of diluting the salinity in BoB. The large excess of freshwater input from rainfall and rivers, compared to loss by evaporation, makes the salinity of the bay far lower compared to the rest of the Indian Ocean. Maintaining a long term steady state condition requires that the excess freshwater be flushed out and water of high salinity flow into the bay. The outflow of low salinity water occurs along its eastern and western boundaries (Behara and Vinayachandran, 2016; Jensen, 2001, 2003) and the inflow of high salinity water (≥ 35 psu) occurs during summer monsoon in the southern BoB (Vinayachandran et al., 2013, 2018). Advection of the high salinity water along with the prevailing circulation and the ensuing mixing is well realized as the principal mechanisms for maintaining the salinity distribution in the BoB (Behara and Vinayachandran, 2016).

Upon entering the BoB, high salinity water continuously evolves and changes its physical properties. A previous study (Singh et al., 2022) used geometric and topological descriptors to track high salinity

water. The study showed that, upon entering BoB, the high salinity water mass splits in three major directions and advances towards Visakhapatnam, the coast of Andaman and Nicobar islands, and the center of BoB. The study was carried out under the assumption that the high salinity water moves northward. Observations of the general trend of movement of high salinity water in the BoB indicate that the assumption is valid. However, the assumption does affect the robustness and applicability of the method to other scenarios. Further, the tracks do not provide additional information regarding the forces or natural phenomenon responsible for the salinity movement, a question of interest to oceanographers. In this paper, we track salinity movement due to ocean currents as compared to other phenomena (diffusion, dispersion, mixing of water). For studying the movement of salinity due to currents, we consider *advection*, which is defined as the mechanical transport of solutes in the fluid along with the movement of the fluid. We design and implement an advection-based tracking method and use it to measure the transport of salinity through BoB due to currents. The tracking method is supported by a definition of physical features in data that is based on advection. The method is used to track the flow of high salinity water in BoB, followed by a comparison against the movement of high salinity water observed using the method of Singh et al.

* Corresponding author.

E-mail addresses: upkarsingh@iisc.ac.in (U. Singh), vinay@iisc.ac.in (P.N. Vinayachandran), vijayn@iisc.ac.in (V. Natarajan).

1.1. Related work

The source of high salinity water in the southern BoB is the high salinity core (HSC) (Vinayachandran et al., 2013, 2018) that intrudes into the bay from the Arabian Sea along with the Summer Monsoon Current (SMC). This water is denser compared to the ambient water, and consequently sinks and then spreads into the rest of the Bay. These movements are affected by the Sri Lanka Dome (SLD) and the path of the SMC. The SLD spins in an anticlockwise direction, upwelling water from below. The SMC generally flows northeastward into the bay and its mean position shifts progressively westward (Vinayachandran and Yamagata, 1998; Webber et al., 2018) with the season along with the HSC. The SMC often consists of eddies (Rath et al., 2019) and splits into multiple branches (George et al., 2019), carrying HSC along with these features. The HSC is located at shallow depths and the property that distinguishes HSC from the BoB is its higher salinity, prompting us to use salinity as the tracer. The large spatial gradients in salinity in the bay (compared to that of temperature) also makes it an ideal tracer for tracking movement of water parcels (Jensen, 2001; Benschila et al., 2014).

The transport of temperature, salt, and other tracers in the ocean from one place to another is carried out to a great extent by advection. Recent studies suggest that ocean heat advection is a dominant process to predict high-latitude ice movement (Nakanowatari et al., 2022). The advection of heat by ocean currents controls the mixed layer heat budget and air–sea interaction in the southern ocean (Gao et al., 2022). In the BoB, advection plays an important role in maintaining the salt and freshwater budgets (Behara and Vinayachandran, 2016; Jensen, 2001, 2003) in addition to controlling the heat budget (Vijith et al., 2020). The circulation patterns in regions close to the coast of Sri Lanka have been studied from various measurements to understand seasonal and year-to-year variations (Pirro et al., 2020; Anutaliya et al., 2022; Rainville et al., 2022).

Effective representation of the HSC and efficient methods for tracking its movement are central to the study of movement of salinity within the BoB. The salinity data is represented as a scalar field defined over a volumetric domain. Geometric and topological approaches towards the representation and tracking of features in scalar field data typically begin with isosurface extraction. An *isosurface* of a scalar field is the preimage of a scalar value. It may consist of multiple connected components, each component enclosing a subvolume. An *isovolume* is the preimage of an interval of scalar values. It is essentially a collection of isosurfaces. The 35 psu isohaline envelopes the HSC in the BoB (Vinayachandran et al., 2013, 2018) and hence the ≥ 35 psu isovolume is used to represent the HSC.

Several methods have been developed within the visualization literature to track and explore spatio-temporal features. Most relevant to the problem of HSC movement tracking are methods that utilize geometric and topological techniques that begin with the assumption that the features of interest are enclosed by individual components of the isosurfaces (Mascarenhas and Snoeyink, 2009). The connectivity of the isosurface over the entire range of scalar values is represented using a topological structure called the Reeb graph, or its variants, such as the contour tree or merge tree (Edelsbrunner and Harer, 2010; Doraiswamy and Natarajan, 2012). A time-varying extension of the Reeb graph (Edelsbrunner et al., 2008) or the contour tree (Sohn and Bajaj, 2006) helps represent the evolution of the entire collection of isosurfaces. Tracks of individual features may be extracted as paths within this time-varying graph. Several other approaches construct a track graph, a directed acyclic graph (DAG) consisting of all potential feature tracks (Bremer et al., 2010; Thomas and Natarajan, 2011; Widanagamaachchi et al., 2012; Doraiswamy et al., 2013; Valsangkar et al., 2019; Pandey et al., 2020; Lukaszczuk et al., 2020). The track graph records the correspondences between features in consecutive time steps by considering the spatial proximity of the critical points that represent the features (Skraba and Wang, 2014; Soler et al., 2018),

spatial overlap (Sohn and Bajaj, 2006; Saikia and Weinkauff, 2017a,b), or by identifying the matches between the subtrees of the contour trees or merge trees (Bremer et al., 2011; Oesterling et al., 2017; Sridharamurthy et al., 2020; Sridharamurthy and Natarajan, 2023).

Other approaches to feature tracking include those based on flow fields (Post et al., 2003), Temperature–Salinity (T–S) diagrams (Talley et al., 2011; Berglund et al., 2017), and transfer functions or color maps for constructing visual representations of time-varying data considered as a 4D scalar field (Tzeng and Ma, 2005). Detection and tracking have also been developed with a focus on individual phenomena such as upwelling (Nascimento et al., 2012, 2015; Artal et al., 2019). Several studies in oceanography are supported by the development of efficient feature tracking methods, as mentioned above (Massey, 2012; Du et al., 2015; Li et al., 2011; Liu et al., 2017; Gad et al., 2018). Xie et al. present a taxonomy of ocean data and related data processing tasks (Xie et al., 2019), including ocean phenomena identification, tracking, and pattern discovery. Afzal et al. survey the task requirements in the context of visual analysis of ocean and atmospheric datasets in Afzal et al. (2019), and discuss different frameworks for data analysis and knowledge discovery.

A recent paper (Singh et al., 2022) introduces two approaches to represent the HSC with a focus on its shape characteristics – a surface front that indicates northward movement and a skeleton that represents overall shape of the volume. The ≥ 35 psu isovolume is a coarse representation of the HSC. The front is defined as a subset of the boundary of the HSC volume. The front-based tracking method computes a boundary surface component of the isovolume with a predisposition to move north. This component is declared as a front and a neighborhood analysis is used to track the front over time. The skeleton-based method aims to capture changes in the shape of the HSC and hence track its movement. It also begins by computing the ≥ 35 psu isovolume. Next, it constructs a skeletal structure (Sato et al., 2000) as a collection of paths in the isovolume. The skeletal structure serves as a descriptor of the isovolume shape, and is tracked over time using a spatial neighborhood analysis.

Both front and skeleton-based representations help track the HSC despite its irregular shape transformations. The front and skeleton-based tracking enables detailed and new observations on the forking behavior of the HSC near the center of the BoB and a long track describing movement towards the coast. The effect of individual ocean dynamics processes like ocean currents, diffusion, and mixing on HSC movement is not studied in these works.

1.2. Contributions

Front and skeleton-based HSC tracking methods (Singh et al., 2022) were used to document the HSC path within the BoB. However, this movement of the HSC is a result of complex ocean dynamics that includes advection, diffusion, and mixing. This paper presents computational methods to study HSC movement that can be attributed to advection. This finer grained analysis helps explain the processes that direct the HSC movement and its path within the BoB. The constantly evolving shape of the HSC, the continuously changing non-uniform distribution of salinity levels within the HSC, and the dynamic current make it difficult to study the effect of advection on the salinity movement. While advection may be directly visualized using pathlines of the velocity field, there exists no clear feature descriptor based on advection to support the finer-grained analysis. The following is a list of key contributions of this paper:

- Introduction of a novel feature of the HSC, called the *advection front*, that helps track its movement as directed by the velocity field.
- Parallel algorithms and methods to compute, track, and analyze the advection front.
- A visual analysis tool to study salinity transport due to advection in the BoB.
- New results and inferences on salinity transport due to ocean currents in the BoB.

2. Data preparation

Data used in this study is from the GLORYS12V1 : Global Ocean Physics Reanalysis repository (Copernicus, 2012). This data is from a reanalysis product and provides multiple fields including salinity, horizontal velocities across latitude and longitude in netCDF format. All fields are available on a 3D rectilinear grid, regularly sampled horizontally with a latitude–longitude resolution of $1/12^\circ$ and irregularly sampled across depth at 50 levels. The data is available at daily resolution for 122 days during the period June 2016–September 2016. We resample the salinity at regular depth levels 1 m apart up to 200 m using linear interpolation. This results in a regular 3D grid data that enables efficient volume processing and visualization.

The data is processed using Climate Data Operators (CDO) command line tools (Schulzweida, 2019) and a geographical region corresponding to the BoB is extracted using bounds on longitude ($75^\circ E$ to $96^\circ E$) and latitude ($5^\circ S$ to $30^\circ N$). The resampling computation is scheduled in parallel, where each pair of consecutive depth slices from the input 3D rectilinear grid is processed concurrently to compute interpolated slices between them. Further, salinity and velocity data is considered only up to a depth of 200 m. HSC movement is observed only in relatively shallow waters (Anutaliya et al., 2017) and hence the restriction. The resulting netCDF file is used for all further processing and analysis. Vertical velocities are not available in the data and need to be estimated based on the available fields.

Vertical velocity estimation. If a fluid is incompressible (such as the ocean water), it satisfies the following equation of continuity (Pond and Pickard, 1983):

$$\frac{\partial u_{p,t}}{\partial x} + \frac{\partial v_{p,t}}{\partial y} + \frac{\partial w_{p,t}}{\partial z} = 0, \quad (1)$$

where $V_{p,t} = (u_{p,t}, v_{p,t}, w_{p,t})$ is the given velocity along x , y , and z axis at a 3D point p in space and at time t . The coordinates are chosen to correspond to longitude, latitude, and depth, respectively. So, the vertical velocity component can be expressed in terms of the horizontal components as

$$\frac{\partial w_{p,t}}{\partial z} = - \left(\frac{\partial u_{p,t}}{\partial x} + \frac{\partial v_{p,t}}{\partial y} \right). \quad (2)$$

When the point p lies at the location of a vertex of the cube grid, it is represented as $p = (x_i, y_j, z_k)$. Here, i, j , and k denote the index of the vertex on the 3D grid. Note that z_k is zero on the ocean surface and negative elsewhere, and $-z_k$ represents the depth below the sea surface. Assuming that the horizontal velocity is available at a total of d depth levels $\{z_1 = 0, z_2, \dots, z_k, \dots, z_d\}$, the vertical velocity at depth $-z_k$ below the surface can be computed as an integral over the slab between layers $z = z_k$ and $z = z_{k-1}$:

$$w_{(x_i, y_j, z_k), t} - w_{(x_i, y_j, z_{k-1}), t} = \int_{z_{k-1}}^{z_k} - \left(\frac{\partial u_{p,t}}{\partial x} + \frac{\partial v_{p,t}}{\partial y} \right) dz. \quad (3)$$

The vertical velocity at depth $-z_{k-1}$ is recursively computed using the integral over the slab between layers $z = z_{k-2}$ and $z = z_{k-1}$, and so on, until the slab whose top layer is the surface of the ocean. The vertical velocity $w_{p,t}$ on the surface of the ocean, namely at depth $z_1 = 0$, is equal to 0. The divergence may be assumed to be a constant within each slab and is set to be equal to the value at the center of the slab, at depth $\frac{1}{2}(z_k + z_{k-1})$. So, the integral is equal to the product of the divergence and the height of the slab. Since the data is available as a discrete sample, the partial derivatives at a given point is estimated as the average of forward and backward differences:

$$\frac{\partial u_{p,t}}{\partial x} = \frac{1}{2} \left(\frac{u_{(x_{i+1}, y_j, z_k), t} - u_{(x_i, y_j, z_k), t}}{D((x_{i+1}, y_j, z_k), (x_i, y_j, z_k))} + \frac{u_{(x_i, y_j, z_k), t} - u_{(x_{i-1}, y_j, z_k), t}}{D((x_i, y_j, z_k), (x_{i-1}, y_j, z_k))} \right) \quad (4)$$

$$\frac{\partial v_{p,t}}{\partial y} = \frac{1}{2} \left(\frac{v_{(x_i, y_{j+1}, z_k), t} - v_{(x_i, y_j, z_k), t}}{D((x_i, y_{j+1}, z_k), (x_i, y_j, z_k))} + \frac{v_{(x_i, y_j, z_k), t} - v_{(x_i, y_{j-1}, z_k), t}}{D((x_i, y_j, z_k), (x_i, y_{j-1}, z_k))} \right) \quad (5)$$

Here, $D()$ is the Euclidean distance between two points in the volume. Each time step is processed independently, resulting in a parallel method for computing $w_{p,t}$. After this computation, we resample the velocity at regular depth levels 1 m apart so that all variables are available on the regular grid mentioned above.

3. Advection and salinity transport

BoB is a complex system of various physical phenomena, many of which influence salinity transport. In previous work (Singh et al., 2022) we studied the overall movement of salinity in BoB, which is the result of all phenomena working in tandem. The surface front tracking based approach to study HSC movement is direct, simple, effective, and amenable to efficient computation. Our objective is to determine the role of advection in salinity transport by comparing the tracks obtained via surface front tracking against those obtained based on advection. An advection-based approach helps us focus on salinity movement caused due to the ocean currents. As mentioned above, the horizontal components of the velocity are available for the region of BoB in the dataset considered in this study. We estimate the vertical velocity component and use it to compute advection.

3.1. Overview

The data consists of a salinity field and a 3D vector field, all sampled over a regular grid. Two components of the vector field are available as input, and the third (vertical) component is computed at grid vertices and interpolated within each cell. The ≥ 35 psu isohaline is a coarse representation of the HSC in the BoB (Vinayachandran et al., 2013, 2018). We incorporate an allowable tolerance ϵ for ocean measurements (Durack and Wijffels, 2010). As a first step, we extract the $35 \pm \epsilon$ psu isovolume (Fig. 1), which serves as an envelope of the high salinity water packets. Subsequent steps focus on computing advection of salinity in this isovolume with the aim of capturing the movement of the HSC due to ocean currents. This is achieved by locating points in the isovolume where the current drives salinity transport, computing clusters of such points, and constructing a graph that consists of tracks of the clusters over time. We introduce a feature representation called advection front, a subset of the $35 \pm \epsilon$ psu isovolume, and track this front across time to determine HSC movement caused by the velocity field. All steps mentioned above can be computed in parallel to improve runtime performance. We first describe the individual steps and discuss the strategy for parallelization later in the section.

3.2. Advection front

Advection is defined as the mechanical transport of solutes due to the movement of solvent. The advection of salinity due to ocean currents at a point p and time t is expressed as

$$A_{p,t} = u_{p,t} \frac{\partial S_{p,t}}{\partial x} + v_{p,t} \frac{\partial S_{p,t}}{\partial y} + w_{p,t} \frac{\partial S_{p,t}}{\partial z}. \quad (6)$$

This analytic expression for advection is applicable for a differentiable salinity function. In practice, the salinity function is available as a sample over a 3D grid. We use the average of the forward and backward difference to estimate the partial derivatives.

$$\frac{\partial S_{p,t}}{\partial x} = \frac{1}{2} \left(\frac{S_{(x_{i+1}, y_j, z_k), t} - S_{(x_i, y_j, z_k), t}}{D((x_{i+1}, y_j, z_k), (x_i, y_j, z_k))} + \frac{S_{(x_i, y_j, z_k), t} - S_{(x_{i-1}, y_j, z_k), t}}{D((x_i, y_j, z_k), (x_{i-1}, y_j, z_k))} \right) \quad (7)$$

$$\frac{\partial S_{p,t}}{\partial y} = \frac{1}{2} \left(\frac{S_{(x_i, y_{j+1}, z_k), t} - S_{(x_i, y_j, z_k), t}}{D((x_i, y_{j+1}, z_k), (x_i, y_j, z_k))} + \frac{S_{(x_i, y_j, z_k), t} - S_{(x_i, y_{j-1}, z_k), t}}{D((x_i, y_j, z_k), (x_i, y_{j-1}, z_k))} \right) \quad (8)$$

$$\frac{\partial S_{p,t}}{\partial z} = \frac{1}{2} \left(\frac{S_{(x_i, y_j, z_{k-1}), t} - S_{(x_i, y_j, z_k), t}}{D((x_i, y_j, z_{k-1}), (x_i, y_j, z_k))} + \frac{S_{(x_i, y_j, z_k), t} - S_{(x_i, y_j, z_{k+1}), t}}{D((x_i, y_j, z_k), (x_i, y_j, z_{k+1}))} \right) \quad (9)$$

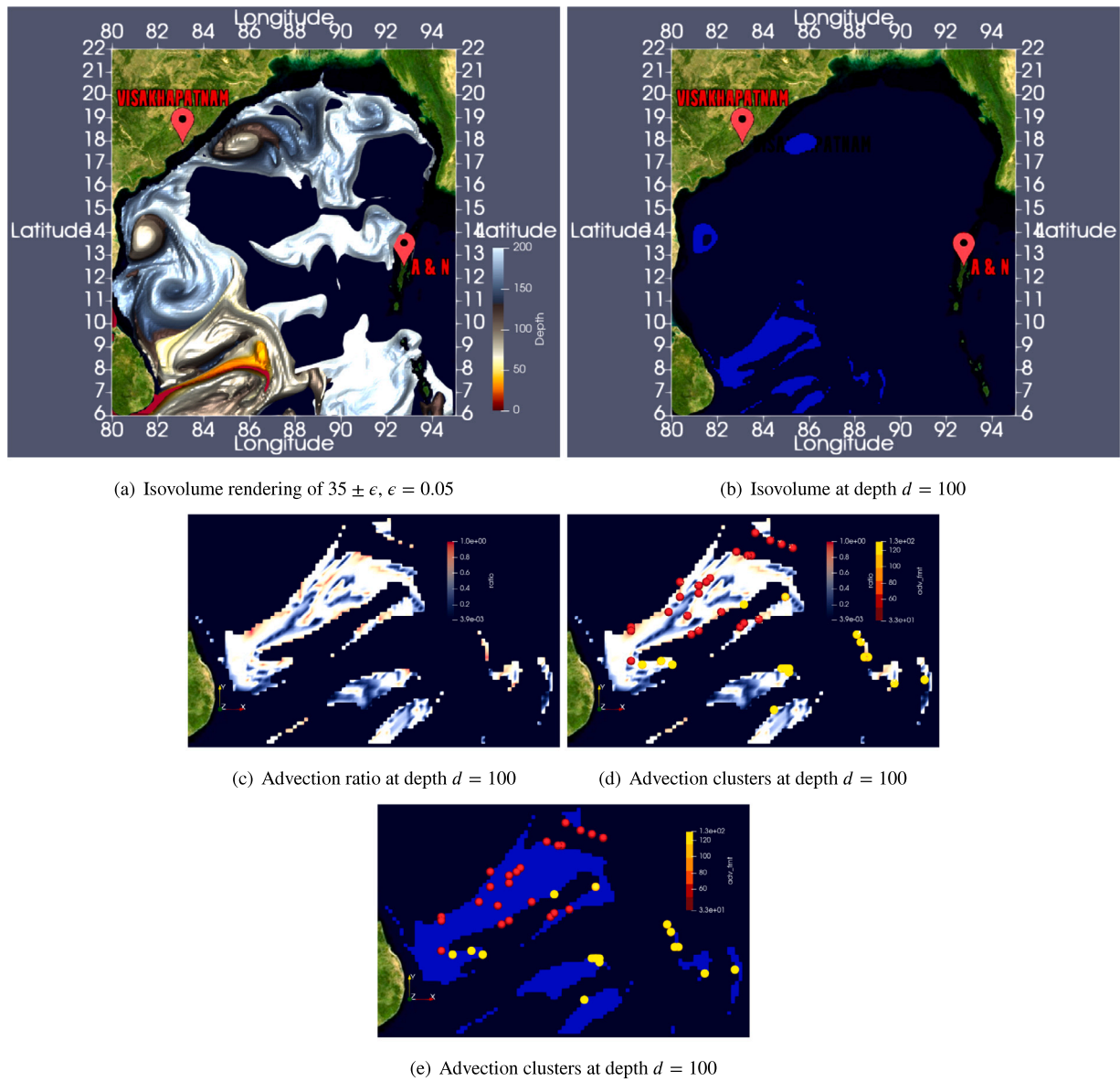


Fig. 1. Advection ratio, points, and clusters. (a) The advection study focuses on the envelope of the high salinity water, which is represented by the $35 \pm \epsilon$ isovolume. (b) Focus on a particular depth slice and a small region in the BoB near Sri Lanka. (c) Advection ratio within the selected region. (d,e) The advection points are identified as those where the advection ratio exceeds a threshold.

Henceforth, we will use the phrase advection to refer to the advection of salinity as expressed above for a discretely sampled salinity function.

Advection point and advection ratio. We use the advection value to locate points in the BoB where the movement of salinity is almost entirely due to ocean current. We characterize such points as those where the advection value is almost equal to the total salinity movement. Define *advection ratio* at a point p as the ratio of magnitude of advection to the magnitude of total salinity movement due to all physical phenomenon at p . The total salinity movement is not equal to the net salinity change over time at p , $\Delta_t(S_{p,t}) = S_{p,t} - S_{p,t+1}$. This is because some of the physical phenomena may oppose each other and the value of total salinity movement may be larger than net salinity change. Total salinity movement at a point is equal to the salinity change due to all physical phenomena, including advection, either supplementing or acting against one other. It is calculated as the sum of absolute values of advection and salinity movement due to other phenomena, $|A_{p,t}| + |\Delta_t(S_{p,t}) - A_{p,t}|$. Therefore, the advection ratio

$$AR_{p,t} = \frac{|A_{p,t}|}{|A_{p,t}| + |\Delta_t(S_{p,t}) - A_{p,t}|}. \quad (10)$$

We use a threshold on this ratio in order to extract the set of advection points. Fig. 1 shows the advection ratio and advection points in a small region within the BoB at depth 100 m. Movement of these advection points in the BoB is a representation of salinity movement due to currents. Our initial experiments with advection points using velocity vectors and pathlines show that advection points tend to move in groups throughout the BoB (see video adv-pathlines accompanying this paper). This observation motivates the idea to track and analyze their movement via these groups.

Advection cluster. We define a feature *advection cluster* as a group of advection points clustered together using a neighborhood criterion. This feature helps represent the movement of advection points as a spatial curve and has a smaller memory footprint when compared to pathlines for the set of all advection points. The cluster is determined using a 3D neighborhood $N_3(p; m)$ of size $m \times m \times m$, a subgrid centered at a point p in the grid consisting of $m^3 - 1$ points. The advection cluster serves as a front for studying and tracking salinity movement due to advection. The surface represented by the collection of points from an

advection cluster is called the *advection front*. We use the terms advection front and advection cluster interchangeably, one representation may be converted into another. Computing the advection fronts plays a key role in capturing the coherent movement of advection points.

Formally, the advection cluster is a maximal set of advection points present in the isovolume of $35 \pm \epsilon$ such that each point in the set lies within the $N_3(p; m)$ neighborhood of at least one other advection point within the cluster. We use a simple connected component labeling method on advection points to compute advection clusters. The advection front is computed as the envelope surface of spheres centered at each point within the corresponding advection cluster. Each advection front $AF_{t,i}$ at time t has a unique label i and can be tracked over time using velocity vectors.

3.3. Track graph

We introduce the *track graph*, a graph that consists of arcs between advection fronts to represent their local movement from one time step to the next. Nodes of the track graph correspond to the advection fronts. An arc between two nodes represents a correspondence between advection fronts from two consecutive time steps. No two advection fronts from the same time step are connected by an arc. The track graph collects all paths followed by the advection fronts over time and serves as a useful data structure to visualize, explore, understand, and analyze the tracks of advection fronts over time. Individual arcs in the graph are computed as follows. For a given advection point p within an advection front $AF_{t,i}$, we compute all points reachable from p following the velocity vector at p . Next, we check if any of these reachable points belongs to the advection front $AF_{t+1,j}$ from the $t+1$ time step. If yes, we have identified a correspondence between $AF_{t,i}$ and $AF_{t+1,j}$ and insert an arc to represent the correspondence.

Nodes with degree-1 represent a creation or termination event, degree-2 nodes represent a continuation event, and degree-3 and higher degree nodes represent a merge/split event. All arcs are directed forward in time and the resulting graph does not contain any cycle. This directed acyclic graph (DAG) is visualized by rendering each node as a point or as a small sphere centered at the advection point closest to the centroid of all points from the cluster. Arcs are rendered as straight line edges between the nodes. This visual representation of tracks helps understand salinity movement.

Since the track graph is a DAG, it contains at least one source and one destination node. The salinity transport due to advection in the BoB is thus captured as the collection of source to destination paths in this track graph. We can extract meaningful paths from this graph for further analysis. In the following, we propose two methods for path extraction from the track graph.

3.4. Advection track

Paths within the track graph are representations of advection front movement. We call them advection tracks. They help locate movements of interest from within the BoB. For example, movement over an extended period of time, movements of large volumes, movements between a specific source and destination, etc. We use two criteria to filter tracks of interest from the track graph: length and source-destination location. Long tracks are indicative of a significant salinity movement due to advection, particularly if the corresponding advection fronts correspond to a large volume of high salinity water. Each arc of the track graph is assigned a cost depending on the desired optimality criterion — say unit cost for lifetime, Euclidean distance between end points for track length, or number of points in the advection clusters for volume spanned by advection front. Optimal cost paths originating at all source nodes are computed using Dijkstra's single source shortest path algorithm. The tracks are binned according to the location of the destination node. Each bin stores the top- k paths and reports them according to user requirements. These tracks together with the advection clusters for each track are stored as a group of VTI files, a Paraview file format, for further analysis and visual exploration in Paraview.

3.5. Parallelism

All time steps are processed concurrently to compute advection and advection ratio, identify advection points, and construct advection clusters. The computations within each time step are independent of each other and hence these time steps may be processed in parallel without any communication. Similarly, a time step t is processed concurrently with other steps to compute arcs of the track graph that originate at t . Each advection point can be independently processed to identify points that are reachable by following the velocity vector and checking whether the reachable points belong to the advection front from time step $t+1$. The advection tracks are computed efficiently using the Dijkstra's single source shortest path algorithm executed concurrently for all source nodes in the track graph.

4. Implementation and visualization tool design

All methods discussed above for processing the data and computing the advection tracks are implemented in Python 3, some execute independently and others within Paraview (Ahrens et al., 2005). The code and scripts are made available in the public domain. Several of the methods are amenable to parallel execution, as discussed above, because the computations depend on local neighborhoods and values. The Python code uses a multiprocessing library for parallel computation across depth levels or across time steps. These concurrent processes do not need to interact with each other. They read data directly from different input files or streams and write outputs into a unique files. So, while different steps required to compute advection tracks are necessarily executed in a serial order, the individual steps are executed in parallel. In this section, we will discuss the implementation of all methods described above. The visualizations are generated using a Python script that execute within Paraview.

4.1. Advection front and track graph

All computations, beginning from data preparation until the construction of the track graph, are implemented in a script `TrackGraph.py`. It resamples the data using linear interpolation on the depth slices, estimates vertical velocities, and uses Numpy (Harris et al., 2020) to extract points in space with salinity value $35 \pm \epsilon$ psu, the required isovolume. Next, it computes advection, advection ratio, advection points, advection clusters, and finally constructs the track graph by identifying individual arcs between advection clusters. The script processes two input files, the GLORYS12V1 data in netCDF format and a parameter file that specifies different thresholds, including the advection ratio, to classify advection points and the value of ϵ for isovolume computation. We discuss the parameter file and its contents later in this section. Data is represented as 2D or 3D matrices in the script and Numpy is used for all arithmetic computations. Numpy provides fast implementations for arithmetic operations on matrices and improves the efficiency of the serial steps. The script uses a smoothing filter and a threshold on minimum size of an advection cluster for noise reduction. The output consists of three groups of files. The first group contains arcs of the track graph, second group stores the advection clusters together with their labels, and the third group stores cluster representatives to be used for visualizing the advection clusters. Finally, a single file in the native VTP format stores the graph so that it can be rendered directly in Paraview.

Theoretically, the size of the track graph can be linear in the number of advection points. The worst case occurs when each cluster contains a single advection point. In practice, a larger number of advection points form a cluster, resulting in a small number of nodes in the track graph. Loading the entire data into main memory may result in low memory availability for each process, and lead to a higher execution time. So, each process spawned by the script loads data from secondary storage as required and releases the memory immediately after use.

4.2. Advection track computation

The groups of files generated by `TrackGraph.py` are processed by the script `LongPaths.py` to extract multiple paths from the track graph. The choice of tracks is governed by a set of parameter values specified in the input parameter file. The paths are grouped based on the location of the source and destination in the BoB. The output consists of a collection of VTP files, one file for each group of paths, which may be rendered using Paraview. The track graph is represented as a DAG using the `DiGraph` data structure from `NetworkX` (Hagberg et al., 2008), which stores the graph as adjacency lists using the dictionary of dictionaries. This “dict-of-dicts” structure allows fast insertion, deletion, and lookup of nodes and neighbors in large graphs, and also supports fast graph algorithms such as shortest path computation, identification of sources and destination in a directed graph. The maximum number of paths within each group is a user-defined parameter. All computations in this script are parallelized across the set of all source nodes by leveraging the fact that the computation of paths from each source is independent of paths from other sources.

4.3. Visualization

The scripts described above store the track graph and paths using data structures from the VTK library that is available with Paraview. Nodes and arcs of the graph in this data structure have associated weights, which may be mapped to colors for useful visualizations. The files containing the track graph are loaded into Paraview and analyzed using builtin filters and colormaps. Paraview supports saving a collection of views to a state file. All visualizations discussed in the results are saved as individual state files and loaded on demand. The state file `trackgraph.pvsm` may be used to visualize the track graph and `tracks.pvsm` for visualizing the track groups.

4.4. Parameter tuning

The `parameter.txt` file contains a list of parameters that the user can specify and tune depending on the user task requirement. The user may specify the name of the input file in the netCDF format together with the spatial resolution as a parameter. The threshold for advection ratio and the value of ϵ are set to default values of 0.95 and 0.05, respectively. They may be edited depending on the requirements of the experiment and data set. The value of the smoothing filter, the minimum size of advection cluster required, and the neighborhood size may also be edited. All experiments in this paper use an $N_3(p; 5)$ neighborhood, which may be edited to any other size (odd number). The user may also edit the parameters used for grouping the paths, namely the specification of the region containing the source and destination of the track and the maximum number of tracks within a group.

5. Results

We now discuss the results of our study of the BoB using the advection-based tracking method described above. We present visualization of the advection tracks and compare them against previously documented observations. We set $\epsilon = 0.05$ and use an advection ratio threshold of 0.95 in all experiments. We choose a small value of ϵ to compute the isovolume while ensuring that the resulting collection of advection points is of considerable size to make meaningful observations. A high advection ratio threshold ensures that salinity movement at advection points may be clearly attributed to advection.

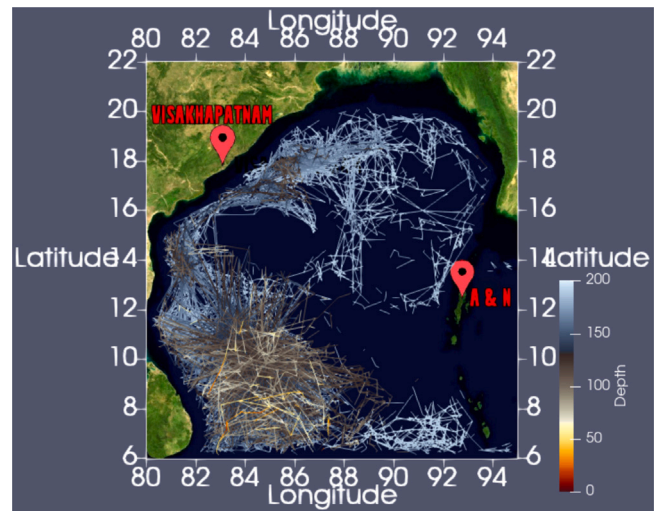


Fig. 2. Track graph representing the collection of all advection tracks in the BoB. Arcs are colored based on their depth. A dense collection of tracks in the south of the BoB at 50 m depth dips down as it moves northward. Fewer tracks appear to progress towards the Andaman and Nicobar islands. Representative tracks may be extracted from this graph to study movements between specific regions in the BoB.

5.1. Salinity advection using pathlines

We first generate a simple pathline based visualization with the aim to study and understand how the ocean current transports salt within the BoB. We extract the $35 \pm \epsilon$ isovolume, compute advection, and identify advection points within the isovolume. A set of seed points are chosen at every 5th time step, pathlines are traced from the seeds for 7 time steps, and the tracing is terminated later. The pathlines provide an overview of the movement of advection points in the BoB, as shown in the video `adv-pathlines` accompanying this paper. Paths are colored based on their depth to better distinguish between shallow and deep advection. We observe that the advection points tend to move in groups and the paths followed by them are similar to those observed in a previous study on HSC movement identification that used a front tracking approach (Singh et al., 2022). Further, their movement is similar to the pathlines generated by selecting all points within the $35 \pm \epsilon$ isovolume as shown in the video `adv-vs-high-salinity-pathlines`. This leads us to a hypothesis that movement of the HSC in the BoB is primarily due to advection and the contribution of diffusion and mixing is small. We aim to verify this hypothesis by computing advection tracks in the BoB and comparing them with the previously observed HSC front tracks.

5.2. Advection tracks

The track graph (Fig. 2) shows a dense collection of paths in the south of BoB at approximately 50 m depth which slowly dips down to a depth range of 150–200 m as they move northward. This is expected as the high salinity water has higher density than the relatively fresh ambient water and slowly slides down as it moves northwards (Vinayachandran et al., 2013). The number of tracks heading towards the coast of the Andaman and Nicobar islands is smaller than those progressing in other directions, which suggests that the advection driven salinity movement towards the Andaman coast is relatively small.

We extract individual advection tracks from the track graph for detailed analysis. Fig. 3 shows a particularly long advection track together with the advection fronts represented by the track over time. The track extends over 60 days, and the figure shows the advection front on every sixth day. The advection front evolves by increasing and decreasing in size as it moves northwards. This may be due to variations

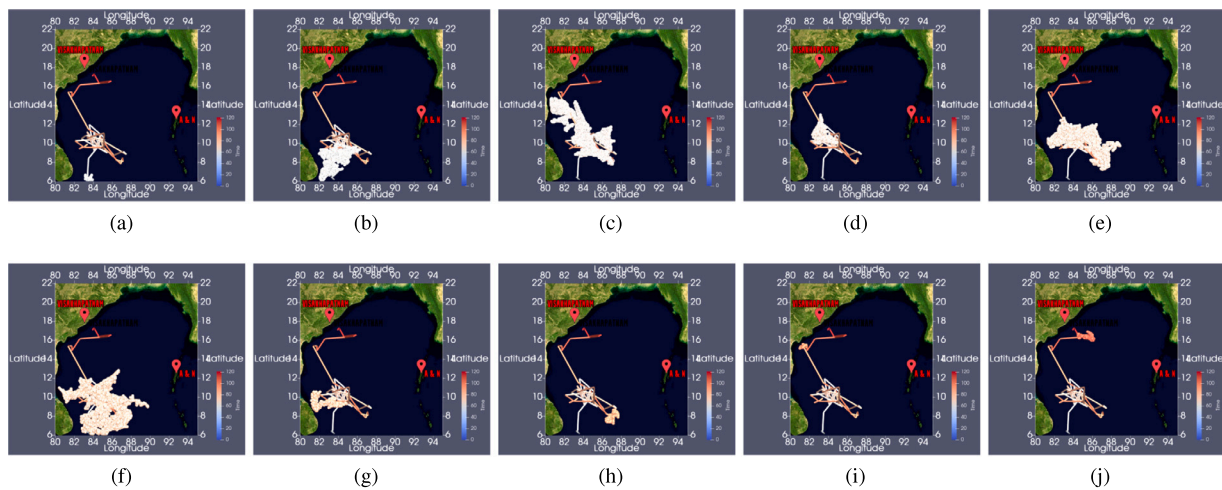


Fig. 3. Advection track and advection fronts. Tracks are displayed using a blue–red color map that indicates time measured in days, ranging from June 1, 2016 (Day 0, blue) to September 30, 2016 (Day 121, red), for a total of 122 time steps (122 days). Nodes of the track are located at the advection point closest to the centroid of the advection cluster in each time step. (a–j) A long advection track that extends approximately 60 days, between July 27 and September 27, provides a visual representation of the movement of advection fronts (shown on every sixth day) towards the coast of India at Visakhapatnam. The size and spatial extent of the advection front evolves over time. The accompanying video shows a split in the advection front in September, which results in the track branching into three directions.

in the velocity. We also observe that the track geometry is tortuous and noisy, which can be fixed by using a post-processing smoothing filter. The video `adv-tracks` accompanying this paper shows three tracks and the corresponding advection fronts. A split in the advection front in August results in the tracks branching into three directions.

Fig. 4 shows five tracks extracted from the track graph. Each track is representative of a group of tracks whose origin and destination are within a common neighborhood. All advection tracks in **Fig. 4** whose origin is in south BoB have a similar structure until they reach the center of BoB. They branch in three directions from the source located near Sri Lanka.

The first and most prominent among them is towards the coast of India, see **Figs. 4(a)** and **4(b)**. Eddies appear to have a major role in the vertical and horizontal movement of the advection tracks along the east coast of India as observed in the video `adv-pathlines`. The analysis shows that the higher salinity water generally sinks to deeper depths of lower velocity regimes and vertical movements are associated with eddies, consistent with existing inferences in the literature. A second branch is in the open bay in a north-eastward direction, see **Fig. 4(d)**. The movement occurs in pulses and thus disconnected from the source at intervals. The third branches towards the east which occurs from the branching of the SMC, see **Fig. 4(c)**.

We also observe some tracks along the Indian coast, which refers to a movement of high salinity water along the coast of India from Visakhapatnam towards north (**Fig. 4(e)**). However, this movement is observed during the month of June (see the color map), before the high-salinity water reaches the coast of Visakhapatnam from the south BoB.

5.3. Advection tracks vs. HSC front-based tracks

We compare the advection tracks against those generated using the HSC front-based method with the aim of testing the hypothesis that advection drives the salinity transport in the BoB. The forking of paths into three major directions near Sri Lanka Dome was also observed in the HSC front-based tracks. Similar to what was observed in the case of advection tracks, one of the branches bends westwards and move towards the coast of India at Visakhapatnam and another bends eastwards and move towards the coast of Andaman and Nicobar islands. One branch continues northward. The HSC front-based tracks were similar to the advection tracks, even in terms of the shape of the tracks. The track located along the Indian east coast is observed in early time steps in both studies.

The qualitative observations above are supported by a quantitative comparison of the tracks obtained by the two methods. Each one of the five representative advection tracks in **Fig. 4** corresponds to a track computed using the HSC front-based method, namely the representative track whose origin and destination lie within the same latitude–longitude interval. We compute the root mean squared error (RMSE) between these pairs of tracks. The RMSE varies between 90 km–115 km, which indicates that the tracks are close to each other. In summary, there is a close match between the tracks in **Fig. 4** and those from the previous study (**Singh et al., 2022, Figure 7**).

Jensen et al. have investigated salinity exchanges between the equatorial Indian Ocean and the BoB, and report that salt is transported northward into the BoB between $83^{\circ}E$ and $95^{\circ}E$ (**Jensen et al., 2016**). Their simulations show a strong subsurface current and an intrusion of high salinity water into the BoB during the southwest and northeast monsoon. This is also in agreement with previous observations of the subsurface intrusion of the southwest monsoon current into the BoB (**Vinayachandran et al., 2013**).

All similarities and strong correlation between the results from advection-based and HSC front-based methods suggest that the salinity movement in the BoB is mostly driven by advection. The contribution of other physical phenomenon, such as mixing and diffusion, in this process is relatively small. One difference is the upward movement towards shallower water near the center of BoB in advection tracks, see **Fig. 4(d,i)**. This was not observed in the HSC front-based tracks (**Singh et al., 2022, Figure 7(b,g)**).

5.4. Performance analysis

The use of the Numpy multiprocessing library for parallel computation results in a considerable speedup of all steps of the method. All experiments are performed on a 32-core Intel Xeon CPU with 386 GB RAM, running Ubuntu Linux. On average, the `TrackGraph.py` script computes the track graph in 16.2 min, compared to 80.7 min using a sequential implementation. Similarly, the script `LongPaths.py` has a running time of 8.36 min, compared to a sequential running time of 28.6 min. The peak memory usage of `TrackGraph.py` is 5 GB and that for `LongPaths.py` is 1 GB. The data is loaded onto main memory only when required and removed subsequently, which may lead to additional secondary memory accesses and potentially larger runtimes. Indeed, there is a trade-off between memory usage and runtime. Faster runtimes are achievable if the entire dataset can be loaded onto main memory.

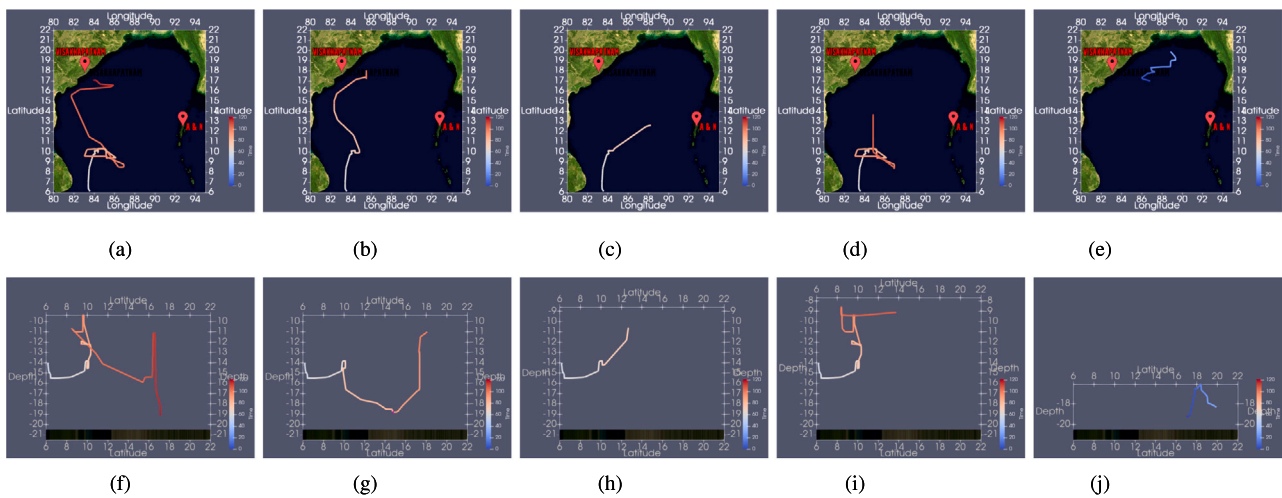


Fig. 4. Five tracks extracted from the track graph that indicate significant movements of the HSC after originating from south BoB and reaching the center of BoB. Tracks are displayed using a blue–red color map that indicates time measured in days, ranging from June 1, 2016 (Day 0, blue) to September 30, 2016 (Day 121, red), for a total of 122 time steps (122 days). (a,b,f,g) Movement towards the coast of India at Visakhapatnam. (c,h) Movement towards the coast of Andaman and Nicobar islands. (d,i) Movement northward from the center of BoB. All movements are observed during the time period between July 27 and September 27 (time steps 56–118). (e,j) A short early movement starting at time step 0 (June 1) along the coast of India. (a,b,c,d,e) Top view. (f,g,h,i,j) Corresponding side view from east.

All intermediate results are stored onto the disk — 56 GB for the interpolated field, 23 GB for storing the advection values, 45 GB for the advection fronts and their labels, and 150 MB for storing arcs of the track graph and the individual tracks. Again, we free memory soon after the intermediate values are processed. The time and space complexity of the algorithm is $O(n)$, where n is the number of points in the input across all time steps. The size of the input can be expressed as $n = t \times d \times l_t \times l_n$, where t , d , l_t , and l_n are number of time steps, depth slices, and dimension in the latitude and longitude, respectively. Each point is accessed a constant number of times.

6. Conclusions

This paper introduced a novel advection front-based method to track the HSC and study its evolution due to the effect of ocean currents. The method is applied to further the study of salinity movement within the BoB. It helped infer the fate of HSC after it enters the southern BoB, subsequent northward movement towards the coast and farther north is directed by advection.

An inflow of high salinity water is required to maintain the salt and freshwater balance of the Bay of Bengal. The major supply of high salinity water into the Bay of Bengal takes place during the summer monsoon. The fate of the HSC after entering the Bay of Bengal has remained largely unknown. Our previous and the present study sheds light on this problem. Analysis of climatological data (Vinayachandran et al., 2013) suggested that the high salinity water progressively dives deeper as it flows northward. Our analysis, on the other hand, suggests that a certain amount of high salinity water flows in the upper layers which has large implications to the maintenance of salinity levels in the Bay of Bengal.

Future work includes the application of the proposed methods towards the study of other water masses such as the North Atlantic Deep Water (Dickson and Brown, 1994) and the flow of Mediterranean Sea Water in the Atlantic Ocean (Richardson et al., 2000). The method is not specific to the BoB and may be applied to other water masses. It requires the user to tune parameter values depending on the data set under consideration and the nature of the study. The value of advection ratio, neighborhood and ϵ are user defined and can be altered to study data from another geographical location. Our algorithm for advection front identification and tracking runs in a shared memory multicore environment and has a reasonably small memory footprint. However, scaling the algorithm to work on higher resolution data and to study salinity movement on a global scale requires the development of distributed parallel methods with a low communication overhead.

Computer code availability

All codes and scripts for computing and tracking features described in this paper are available at https://bitbucket.org/vgl_iisc/bob-salinity-visualization.

CRediT authorship contribution statement

Upkar Singh: Methodology - advection points, Advection cluster computation and visual analysis, Investigation, Visualization, Software, Writing – original draft. **P.N. Vinayachandran:** Conceptualization, Writing – review & editing. **Vijay Natarajan:** Conceptualization, Methodology, Writing – review & editing.

Declaration of competing interest

The authors declare that they have no known competing financial interests or personal relationships that could have appeared to influence the work reported in this paper.

Data availability

Link to the data repository is included in the article.

Acknowledgments

This study was funded by a grant from SERB, Govt. of India (CRG/2021/005278). US is supported by a scholarship from MoE, Govt. of India. PNV acknowledges partial support from National Supercomputing Mission, DST, and the J. C. Bose Fellowship awarded by the SERB, DST, Govt. of India. VN acknowledges support from the Alexander von Humboldt Foundation and from Berlin MATH+ under the Visiting Scholar program. Part of this work was completed when VN was a guest Professor at the Zuse Institute Berlin.

Appendix A. Supplementary data

Supplementary material related to this article can be found online at <https://doi.org/10.1016/j.cageo.2023.105493>.

References

- Afzal, S., Hittawe, M.M., Ghani, S., Jamil, T., Knio, O., Hadwiger, M., Hoteit, I., 2019. The state of the art in visual analysis approaches for ocean and atmospheric datasets. *Comput. Graph. Forum* 38 (3), 881–907.
- Ahrens, J., Geveci, B., Law, C., 2005. Paraview: An end-user tool for large data visualization. In: *The Visualization Handbook*. 717, Elsevier München.
- Anutaliya, A., Send, U., McClean, J., Sprintall, J., Lankhorst, M., Lee, C., Rainville, L., Priyadarshani, W., Jinadasa, S., 2022. Seasonal and year-to-year variability of boundary currents and eddy salt flux along the eastern and southern coasts of Sri Lanka observed by PIES and satellite measurements. *J. Phys. Oceanogr.* 52 (12), 3015–3031.
- Anutaliya, A., Send, U., McClean, J.L., Sprintall, J., Rainville, L., Lee, C.M., Jinadasa, S.U.P., Wallcraft, A.J., Metzger, E.J., 2017. An undercurrent off the east coast of Sri Lanka. *Ocean Sci.* 13 (6), 1035–1044. <http://dx.doi.org/10.5194/os-13-1035-2017>, URL <https://os.copernicus.org/articles/13/1035/2017/>.
- Artal, O., Sepúlveda, H.H., Mery, D., Pieringer, C., 2019. Detecting and characterizing upwelling filaments in a numerical ocean model. *Comput. Geosci.* 122, 25–34.
- Behara, A., Vinayachandran, P.N., 2016. An OGCM study of the impact of rain and river water forcing on the Bay of Bengal. *J. Geophys. Res.: Oceans* 121 (4), 2425–2446.
- Benshila, R., Durand, F., Masson, S., Bourdallé-Badie, R., de Boyer Montégut, C., Papa, F., Madec, G., 2014. The upper Bay of Bengal salinity structure in a high-resolution model. *Ocean Model.* 74, 36–52.
- Berglund, S., Döös, K., Nycander, J., 2017. Lagrangian tracing of the water–mass transformations in the atlantic ocean. *Tellus A* 69, 1306311. <http://dx.doi.org/10.1080/16000870.2017.1306311>.
- Bremer, P., Weber, G., Pascucci, V., Day, M., Bell, J., 2010. Analyzing and tracking burning structures in lean premixed hydrogen flames. *IEEE Trans. Vis. Comput. Graphics* 16 (2), 248–260. <http://dx.doi.org/10.1109/TVCG.2009.69>.
- Bremer, P.-T., Weber, G., Tierny, J., Pascucci, V., Day, M., Bell, J., 2011. Interactive exploration and analysis of large-scale simulations using topology-based data segmentation. *IEEE Trans. Vis. Comput. Graphics* 17 (9), 1307–1324.
- Copernicus, 2012. GLORYS12V1 : Global Ocean Physics Reanalysis. Real-time global forecasting CMEMS system, <http://dx.doi.org/10.48670/moi-00021>.
- Dickson, R.R., Brown, J., 1994. The production of North Atlantic deep water: Sources, rates, and pathways. *J. Geophys. Res.: Oceans* 99 (C6), 12319–12341. <http://dx.doi.org/10.1029/94JC00530>, arXiv:<https://agupubs.onlinelibrary.wiley.com/doi/pdf/10.1029/94JC00530>, URL <https://agupubs.onlinelibrary.wiley.com/doi/abs/10.1029/94JC00530>.
- Doraiswamy, H., Natarajan, V., 2012. Computing Reeb graphs as a union of contour trees. *IEEE Trans. Vis. Comput. Graphics* 19 (2), 249–262.
- Doraiswamy, H., Natarajan, V., Nanjundiah, R.S., 2013. An exploration framework to identify and track movement of cloud systems. *IEEE Trans. Vis. Comput. Graphics* 19 (12), 2896–2905. <http://dx.doi.org/10.1109/TVCG.2013.131>.
- Du, Z., Fang, L., Bai, Y., Zhang, F., Liu, R., 2015. Spatio-temporal visualization of air–sea CO₂ flux and carbon budget using volume rendering. *Comput. Geosci.* 77, 77–86.
- Durack, P.J., Wijffels, S.E., 2010. Fifty-year trends in global ocean salinities and their relationship to broad-scale warming. *J. Clim.* 23 (16), 4342–4362.
- Edelsbrunner, H., Harer, J., 2010. *Computational Topology - An Introduction*. American Mathematical Society.
- Edelsbrunner, H., Harer, J., Mascarenhas, A., Pascucci, V., Snoeyink, J., 2008. Time-varying Reeb graphs for continuous space–time data. *Comput. Geometry* 41 (3), 149–166.
- Gad, M.A., Elshehaly, M.H., Gračanin, D., Elmongui, H.G., 2018. A tracking analyst for large 3D spatiotemporal data from multiple sources (case study: Tracking volcanic eruptions in the atmosphere). *Comput. Geosci.* 111, 283–293.
- Gao, Y., Kamenkovich, I., Perlin, N., Kirtman, B., 2022. Oceanic advection controls mesoscale mixed layer heat budget and air–sea heat exchange in the southern ocean. *J. Phys. Oceanogr.* 52 (4), 537–555.
- George, J.V., Vinayachandran, P.N., Vijith, V., Thushara, V., Nayak, A.A., Pargaonkar, S.M., Amol, P., Vijaykumar, K., Matthews, A.J., 2019. Mechanisms of barrier layer formation and erosion from in situ observations in the Bay of Bengal. *J. Phys. Oceanogr.* 49 (5), 1183–1200. <http://dx.doi.org/10.1175/JPO-D-18-0204.1>, URL <https://journals.ametsoc.org/view/journals/phoc/49/5/jpo-d-18-0204.1.xml>.
- Hagberg, A., Swart, P., Schult, D., 2008. *Exploring Network Structure, Dynamics, and Function Using NetworkX*. Technical Report, Los Alamos National Lab.(LANL), Los Alamos, NM (United States).
- Harris, C.R., Millman, K.J., van der Walt, S.J., Gommers, R., Virtanen, P., Cournapeau, D., Wieser, E., Taylor, J., Berg, S., Smith, N.J., Kern, R., Picus, M., Hoyer, S., van Kerkwijk, M.H., Brett, M., Haldane, A., del Río, J.F., Wiebe, M., Peterson, P., Gérard-Marchant, P., Sheppard, K., Reddy, T., Weckesser, W., Abbasi, H., Gohlke, C., Oliphant, T.E., 2020. Array programming with NumPy. *Nature* 585 (7825), 357–362. <http://dx.doi.org/10.1038/s41586-020-2649-2>.
- Jensen, T.G., 2001. Arabian sea and Bay of Bengal exchange of salt and tracers in an ocean model. *Geophys. Res. Lett.* 28 (20), 3967–3970.
- Jensen, T.G., 2003. Cross-equatorial pathways of salt and tracers from the northern Indian ocean: Modelling results. *Deep Sea Res. Part II: Top. Stud. Oceanogr.* 50 (12–13), 2111–2127.
- Jensen, T.G., Wijesekera, H.W., Nyadjro, E.S., Thoppil, P.G., Shriver, J.F., Sandeep, K., Pant, V., 2016. Modeling salinity exchanges between the equatorial Indian ocean and the Bay of Bengal. *Oceanography* 29 (2), 92–101.
- Li, W., Chen, G., Kong, Q., Wang, Z., Qian, C., 2011. A VR-ocean system for interactive geospatial analysis and 4D visualization of the marine environment around antarctica. *Comput. Geosci.* 37 (11), 1743–1751.
- Liu, S., Chen, G., Yao, S., Tian, F., Liu, W., 2017. A framework for interactive visual analysis of heterogeneous marine data in an integrated problem solving environment. *Comput. Geosci.* 104, 20–28.
- Lukaszczuk, J., Garth, C., Weber, G.H., Biedert, T., Maciejewski, R., Leitte, H., 2020. Dynamic nested tracking graphs. *IEEE Trans. Vis. Comput. Graphics* 26 (1), 249–258. <http://dx.doi.org/10.1109/TVCG.2019.2934368>.
- Mascarenhas, A., Snoeyink, J., 2009. Isocontour based visualization of time-varying scalar fields. In: *Mathematical Foundations of Scientific Visualization, Computer Graphics, and Massive Data Exploration*. Springer, pp. 41–68.
- Massey, N., 2012. Feature tracking on the hierarchical equal area triangular mesh. *Comput. Geosci.* 44, 42–51.
- Nakanowatari, T., Inoue, J., Zhang, J., Watanabe, E., Kuroda, H., 2022. A new norm for seasonal sea ice advance predictability in the Chukchi sea: Rising influence of ocean heat advection. *J. Clim.* 35 (9), 2723–2740.
- Nascimento, S., Casca, S., Mirkin, B., 2015. A seed expanding cluster algorithm for deriving upwelling areas on sea surface temperature images. *Comput. Geosci.* 85, 74–85.
- Nascimento, S., Franco, P., Sousa, F., Dias, J., Neves, F., 2012. Automated computational delimitation of SST upwelling areas using fuzzy clustering. *Comput. Geosci.* 43, 207–216.
- Oesterling, P., Heine, C., Weber, G., Morozov, D., Scheuermann, G., 2017. Computing and visualizing time-varying merge trees for high-dimensional data. In: Carr, H., Garth, C., Weinkauff, T. (Eds.), *Topological Methods in Data Analysis and Visualization IV: Theory, Algorithms, and Applications*. Springer, pp. 87–101.
- Pandey, K., Monteiro, J.M., Natarajan, V., 2020. An integrated geometric and topological approach for the identification and visual analysis of Rossby wave packets. *Mon. Weather Rev.* 148 (8), 3139–3155. <http://dx.doi.org/10.1175/MWR-D-20-0014.1>, URL <https://journals.ametsoc.org/view/journals/mwr/148/8/mwrD200014.xml>.
- Pirro, A., Wijesekera, H., Jarosz, E., Fernando, H., 2020. Dynamics of intraseasonal oscillations in the Bay of Bengal during summer monsoons captured by mooring observations. *Deep Sea Res. Part II: Top. Stud. Oceanogr.* 172, 104718.
- Pond, S., Pickard, G.L., 1983. *Introductory Dynamical Oceanography*. Gulf Professional Publishing.
- Post, F.H., Vrolijk, B., Hauser, H., Laramée, R.S., Doleisch, H., 2003. The state of the art in flow visualisation: Feature extraction and tracking. *Comput. Graph. Forum* 22 (4), 775–792.
- Rainville, L., Lee, C.M., Arulanathan, K., Jinadasa, S., Fernando, H.J., Priyadarshani, W., Wijesekera, H., 2022. Water mass exchanges between the Bay of Bengal and Arabian Sea from multiyear sampling with autonomous gliders. *J. Phys. Oceanogr.* 52 (10), 2377–2396.
- Rao, R., Sivakumar, R., 2003. Seasonal variability of sea surface salinity and salt budget of the mixed layer of the north Indian ocean. *J. Geophys. Res.: Oceans* 108 (C1), 3009:1–14.
- Rath, S., Vinayachandran, P.N., Behara, A., Neema, C., 2019. Dynamics of summer monsoon current around Sri Lanka. *Ocean Dyn.* 69 (10), 1133–1154.
- Richardson, P., Bower, A., Zenk, W., 2000. A census of meddies tracked by floats. *Prog. Oceanogr.* 45 (2), 209–250. [http://dx.doi.org/10.1016/S0079-6611\(99\)00053-1](http://dx.doi.org/10.1016/S0079-6611(99)00053-1), URL <https://www.sciencedirect.com/science/article/pii/S0079661199000531>.
- Saikia, H., Weinkauff, T., 2017a. Fast topology-based feature tracking using a directed acyclic graph. In: *Topological Methods in Data Analysis and Visualization*. Springer, pp. 155–169.
- Saikia, H., Weinkauff, T., 2017b. Global feature tracking and similarity estimation in time-dependent scalar fields. *Comput. Graph. Forum* 36 (3), 1–11.
- Sato, M., Bitter, I., Bender, M.A., Kaufman, A.E., Nakajima, M., 2000. TEASAR: Tree-structure extraction algorithm for accurate and robust skeletons. In: *Proc. Pacific Conf. Computer Graphics and Applications*. pp. 281–449.
- Schulzweida, U., 2019. CDO user guide. <http://dx.doi.org/10.5281/zenodo.3539275>.
- Shetye, S., Gouveia, A., Shankar, D., Shenoi, S., Vinayachandran, P.N., Sundar, D., Michael, G., Nampoothiri, G., 1996. Hydrography and circulation in the western Bay of Bengal during the northeast monsoon. *J. Geophys. Res.: Oceans* 101 (C6), 14011–14025.
- Singh, U., Dhipu, T., Vinayachandran, P.N., Natarajan, V., 2022. Front and skeleton features based methods for tracking salinity propagation in the ocean. *Comput. Geosci.* 159, 104993.
- Skraba, P., Wang, B., 2014. Interpreting feature tracking through the lens of robustness. In: *Topological Methods in Data Analysis and Visualization III*. Springer, pp. 19–37.
- Sohn, B.-S., Bajaj, C., 2006. Time-varying contour topology. *IEEE Trans. Vis. Comput. Graphics* 12 (1), 14–25.
- Soler, M., Plainchaud, M., Conche, B., Tierny, J., 2018. Lifted Wasserstein matcher for fast and robust topology tracking. In: *2018 IEEE 8th Symposium on Large Data Analysis and Visualization. Lдав, IEEE*, pp. 23–33.
- Sridharamurthy, R., Masood, T.B., Kamakshidasan, A., Natarajan, V., 2020. Edit distance between merge trees. *IEEE Trans. Vis. Comput. Graphics* 26 (03), 1518–1531.
- Sridharamurthy, R., Natarajan, V., 2023. Comparative analysis of merge trees using local tree edit distance. *IEEE Trans. Vis. Comput. Graphics* 29 (02), 1518–1530.

- Talley, L., Pickard, G., Emery, W., Swift, J., 2011. *Descriptive Physical Oceanography: An Introduction*, sixth ed. pp. 1–555.
- Thomas, D.M., Natarajan, V., 2011. Symmetry in scalar field topology. *IEEE Trans. Vis. Comput. Graphics* 17 (12), 2035–2044.
- Tzeng, F.-Y., Ma, K.-L., 2005. Intelligent feature extraction and tracking for visualizing large-scale 4D flow simulations. In: SC '05: Proceedings of the 2005 ACM/IEEE Conference on Supercomputing. p. 6. <http://dx.doi.org/10.1109/SC.2005.37>.
- Valsangkar, A.A., Monteiro, J.M., Narayanan, V., Hotz, I., Natarajan, V., 2019. An exploratory framework for cyclone identification and tracking. *IEEE Trans. Vis. Comput. Graphics* 25 (3), 1460–1473. <http://dx.doi.org/10.1109/TVCG.2018.2810068>.
- Vijith, V., Vinayachandran, P.N., Webber, B.G., Matthews, A.J., George, J.V., Kanaujia, V.K., Lotliker, A.A., Amol, P., 2020. Closing the sea surface mixed layer temperature budget from in situ observations alone: Operation advection during BoBBLE. *Sci. Rep.* 10 (1), 1–12.
- Vinayachandran, P.N., Matthews, A.J., Kumar, K.V., Sanchez-Franks, A., Thushara, V., George, J., Vijith, V., Webber, B.G., Queste, B.Y., Roy, R., et al., 2018. BoBBLE: Ocean–atmosphere interaction and its impact on the South Asian monsoon. *Bull. Am. Meteorol. Soc.* 99 (8), 1569–1587.
- Vinayachandran, P.N., Shankar, D., Vernekar, S., Sandeep, K.K., Amol, P., Neema, C.P., Chatterjee, A., 2013. A summer monsoon pump to keep the Bay of Bengal salty. *Geophys. Res. Lett.* 40 (9), 1777–1782. <http://dx.doi.org/10.1002/grl.50274>, URL <https://agupubs.onlinelibrary.wiley.com/doi/abs/10.1002/grl.50274>.
- Vinayachandran, P.N., Yamagata, T., 1998. Monsoon response of the sea around Sri Lanka: Generation of thermal domes and anticyclonic vortices. *J. Phys. Oceanogr.* 28 (10), 1946–1960.
- Webber, B.G., Matthews, A.J., Vinayachandran, P.N., Neema, C., Sanchez-Franks, A., Vijith, V., Amol, P., Baranowski, D.B., 2018. The dynamics of the Southwest Monsoon current in 2016 from high-resolution in situ observations and models. *J. Phys. Oceanogr.* 48 (10), 2259–2282.
- Widanagamaachchi, W., Christensen, C., Pascucci, V., Bremer, P., 2012. Interactive exploration of large-scale time-varying data using dynamic tracking graphs. In: *IEEE Symp. Large Data Analysis and Visualization. LDAV*, pp. 9–17. <http://dx.doi.org/10.1109/LDAV.2012.6378962>.
- Xie, C., Li, M., Wang, H., Dong, J., 2019. A survey on visual analysis of ocean data. *Visual Inf.* 3 (3), 113–128.